THE JOURNAL OF PHYSICAL CHEMISTRY Letters

pubs.acs.org/JPCL Letter

Pressure-Driven Transformation of $CsPbBrI_2$ Nanoparticles into Stable Nanosheets in Solution through Self-Assembly

Yongqiang Ji, Minqiang Wang,* Zhi Yang, Hengwei Qiu, Song Kou, Muhammad Amin Padhiar, Arshad Saleem Bhatti, and Nikolai V. Gaponenko

Cite This: *J. Phys. Chem. Lett.* 2020, 11, 9862−9868 Read Online

ACCESS | Metrics & More | Article Recommendations | Supporting Information

ABSTRACT: Very recently, two-dimensional (2D) perovskite nanosheets (PNSs), taking the advantages of perovskite as well as the 2D structure properties, have received an enormous level of interest throughout the scientific community. In spite of this incredible success in perovskite nanocrystals (NCs), self-assembly of many nanostructures in metal halide perovskites has not yet been realized, and producing highly efficient red-emitting PNSs remains challenging. In this Letter, we show that by using $CsPbBrI_2$ perovskite nanoparticles (NPs) as a building block, PNSs can emerge spontaneously under high ambient pressure via template-free self-assembly without additional complicated operation. It is found that the formation of PNSs is ascribed to the high pressure that provides the driving force for the alignment of NPs in solution. Because of the disappearance of the grain boundaries between the adjacent NPs and increased crystallinity, these PNSs self-assembled from NPs exhibit enhanced properties compared to the initial NPs, including higher PL intensity and remarkable chemical stability toward light and water.

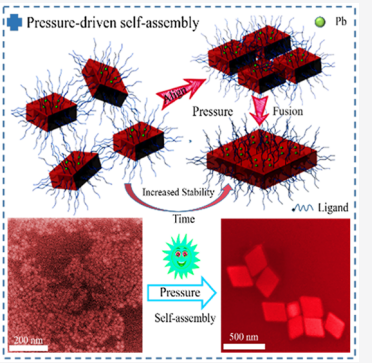

Over a relatively short period of time, interest in metal trihalide perovskite NCs has grown remarkably throughout the scientific community because of their excellent optical properties.[1−6] In particular, this is because of their extremely sharp emission with high photoluminescence quantum yields (PLQYs) as well as composition and size-related luminescence characteristics covering the entire visible spectrum. Perovskite NCs are attractive candidates not only for basic research but also for device applications, such as light-emitting diodes, solar cells, and lasers.[7−11] In spite of this incredible success in perovskite NCs, the self-assembly of many metal trihalide perovskite nanostructures has not yet been realized, and the production of efficient red-emitting perovskite nanosheets (PNSs) is still challenging. In addition, instability of perovskite NCs is manifested as the decrease of luminescence performance under the influence of light, humidity, and heat, which is still an urgent problem to be solved.[12−15]

Very recently, 2D PNSs, taking the advantages of perovskite as well as the 2D structure properties, are more compatible with the conventional thin-film fabrication techniques, which extends them to substantially wider application domains.[16−19] Despite there being successful methods from the last five years to fabricate PNSs, such as the work reported by our group,[16] it usually requires very careful and strict operation. In addition to the synthesis method of PNSs, fundamental insights for the self-assembly of PNSs is still unclear, with only a few groups dealing with this issue.[20,21] Self-assembly from individual building blocks to larger structures is considered to be a promising strategy for the improvement optoelectronic properties of perovskite NCs.[22−26] Indeed, their properties can be further enhanced by the hierarchical arrangement of individual NPs, endowing the self-assembled structures with superior collective properties over individual NCs. For example, another one of our contributions confirmed that nanocubes can self-assemble into 1D supercrystals with improved stability.[25] External perturbation, such as polar solvents, heat, light, and electron beam, usually cause the decomposition of the perovskite NCs; contrary to this common-place observation, recent studies have shown that if external perturbation is used properly, it can drive perovskite NC self-assemble into supercrystals with novel properties.[27−31] For example, Sun et al. found that polar solvents can induce nanocubes to transform into single-crystalline nanowires,[27] and later, light irradiation also successfully induced the self-assembly of $CsPbBr_3$ nanocubes into nanowires or supercrystals, exhibiting enhanced properties.[29,31] However, to our best knowledge, the self-assembly of NPs into PNSs driven by ambient pressure remains largely unexplored, especially in red-emitting PNSs.

In this Letter, physical insights of pressure-induced $CsPbBrI_2$ NPs to PNSs formation in solution are reported. Analysis suggested that NPs are self-assembled in two dimensions, and

Received: September 9, 2020
Accepted: October 28, 2020

https://dx.doi.org/10.1021/acs.jpclett.0c02747
J. Phys. Chem. Lett. 2020, 11, 9862−9868

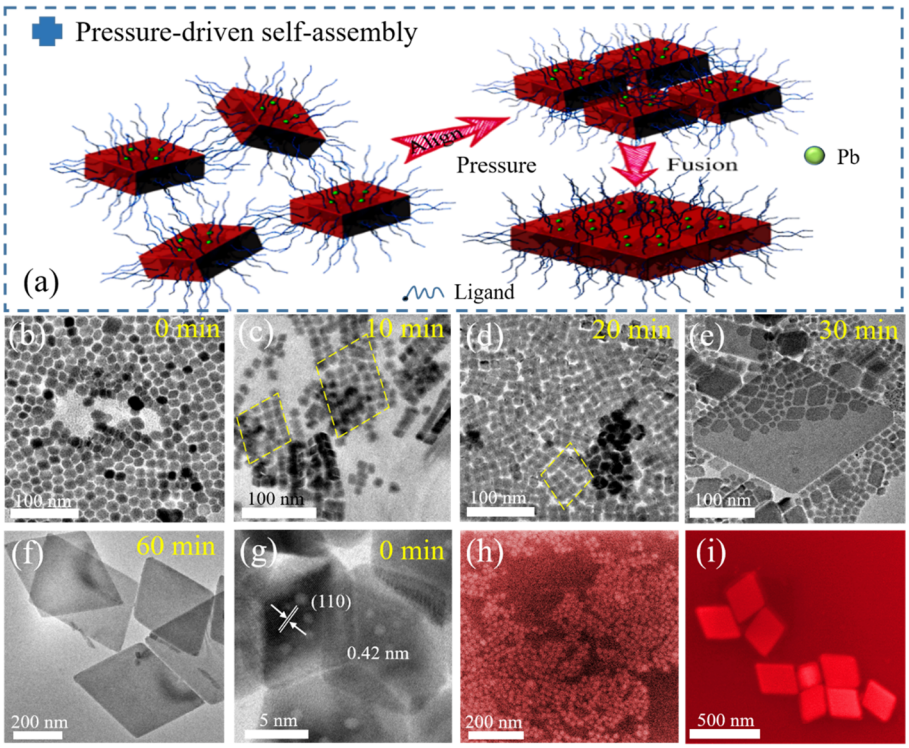

Figure 1. (a) Schematic diagram of NP self-assembly into NPSs under high ambient pressure. (b–i) TEM and SEM images of NPs and PNSs. (b and h) Initial NPs, (c) 2D array formed after 10 min, (d) PNS prototypes formed after 20 min, (e) PNSs formed after 30 min, and (f, and i) PNSs completely formed after 60 min. (g) HRTEM image of initial NPs.

these were further converted to single-crystal PNSs. Because of the disappearance of the grain boundaries and increased crystallinity, these PNSs self-assembled from NPs exhibit enhanced PL intensity and remarkable chemical stability toward light and stability.

These $CsPbBrI_2$ NPs were prepared by modifying the reaction conditions initially adopted by Protesescu et al.[1] Namely, both precursors are obtained in air, then preheated to the desired temperature, and finally mixed for reaction, as displayed in Figure S1. The product observed by transmission electron microscopy (TEM) displays monodisperse NPs with smooth outer surfaces and sharp edges (Figure 1b,h), including some cuboid-like NPs. Well-resolved lattice fringes from high-resolution TEM (HRTEM) images are measured to be 0.42 nm (Figure 1g), consistent with the value of the (110) plane of cubic perovskite NCs.[25] These cuboid-like NPs were also obtained by Rogach's group through the self-assembly of tiny nanoplatelets, but very careful and strict operations are required.[32] Subsequently, these NPs were transferred into a Teflon-lined stainless-steel autoclave for pressure-driven self-assembly reaction (Figure S2). To track the details of shape evolution, the intermediates of PNSs were examined by monitoring the TEM images collected at different stages. Generally, the initial NP surfaces are usually covered with large amounts of ligands. After being treated for 10 min, the pressure of the reaction system increases, the isotropic pressure uniformly applied to the NPs component in all directions causes the size of the unit cell to shrink uniformly,[33] and ligands adsorbed on the surface of NPs start to be removed, mainly because the binding energies of the surface ligands are not sufficiently large to avoid deformation under high ambient pressure, resulting in the reduction of the steric repulsion generated by the ligands.[29] At the same time, the surfaces of $CsPbBrI_2$ NPs are exposed, which is a necessary condition for lattice match and subsequent oriented-attachment growth (Figure 1a). After the removal of the surface ligands under high ambient pressure, the interspacing of adjacent NPs first decreases; these NPs spontaneously align and arrange (Figure 1c) and then gradually tend to form 2D arrays, and finally lattice matching and fusing to NS prototypes with the contour of a parallelogram, but the contours of NPs still can be clearly seen (Figure 1d). At the same time, the surface ligands are squeezed out when the assembly process goes forward accompanied by fusing of NCs; more and more PNSs begin to appear although at various sizes because of different rates of assembly, but some small NPs and intermediates still exist (Figure 1e), which strongly support the self-assembly growth process where, at the early stages of self-assembly, these NPs as building blocks are involved.[34] The driving force for the alignment of $CsPbBrI_2$ NPs is believed to be dipole–dipole interactions, which have been reported in metal halide perovskite systems.[27] As the reaction proceeds, all NCs completely transform into PNSs (Figure 1f,i). According to the characteristics of the Teflon-lined stainless-steel autoclave, the pressure range of the system is about 10 MPa, which is much smaller than the driving pressure of $CsPbBr_3$ reported by Nagaoka et al.[33] This may be because the $CsPbBrI_2$ NCs are more sensitive to pressure and can be driven at a lower pressure to achieve self-assembly. To make this assembly a more complete story, we have also added more intermediate state of assembly data in Figures S3 and S4. We also observed the detailed crystallographic structure in which adjacent NPs have the same lattice spacing of 0.42 nm, even in the regions where they are connected (Figure S5), confirming the existence of lattice matching during the self-assembly process.

https://dx.doi.org/10.1021/acs.jpclett.0c02747
J. Phys. Chem. Lett. 2020, 11, 9862–9868

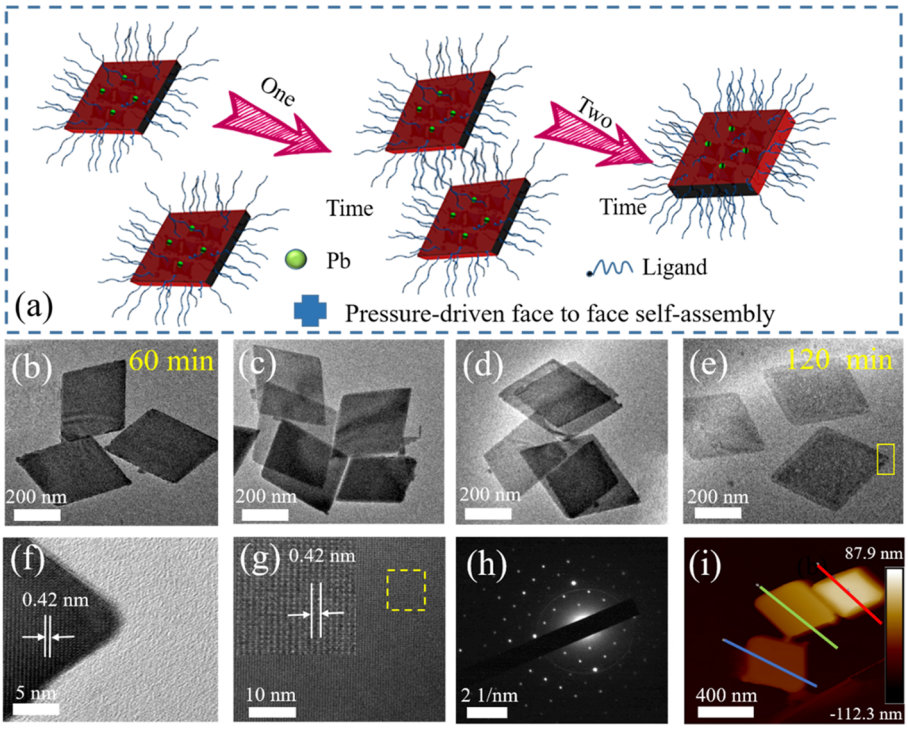

Figure 2. (a) Schematic illustration of pressure-driven face-to-face self-assembly process of PNSs. (b–e) TEM images illustration of pressure-driven face-to-face self-assembly process of PNSs. (f) HRTEM images of thick NS edge. (g) HRTEM images inside thick NS. (h) SAED pattern of thick NS. (i) AFM image of thick PNSs.

In the following, we illustrate the higher-quality PNSs synthesized by our approach, which is facile and applicable. It can be found that the product tends to resemble a parallelogram rather than a cube in shape with edge lengths of 300–400 nm, including some rare PNSs that exhibit a somewhat more rhombic morphology (Figure S6a, b), significantly more uniform than that of parallelogram PNSs reported previously by Zhang et al.,[35] who could get parallelogram PNSs with a length of ∼60–250 nm, and later, the lattice spacing measured from HRTEM is 0.42 nm (Figure S6c), corresponding to the (110) crystal lattice planes of cubic perovskite NCs. The same distance as the lattice fringes in the body of the NCs, suggesting that the NPs coalesced together via an oriented-attachment mechanism rather than through Ostwald ripening. Figure S6d presents the selected area electron diffraction (SAED) pattern, recorded by directing the electron beam perpendicular to the surface of a single NS. The squared sets of spots support the high crystallinity of PNSs, which is also consistent with the scenario reported by Fu et al.[36] Smooth surfaces and edges of the PNSs are observed from the SEM image on the Si substrate (Figure 1i). Subsequently, the element mapping images recorded the signal NS in the nanoprobe mode, indicating that Cs (green), Pb (pink), Br (light-yellow), and I (red) elements are uniformly distributed throughout the whole NS (Figure S6f–k), and the ratio of Cs/Pb/Br/I in energy-dispersive X-ray spectroscopy (EDS) is about 23.51/16.08/19.86/40.55, which is in good agreement with the composition of $CsPbBrI_2$ (Figure S7a). Atomic force microscopy (AFM) was used to characterize the morphological properties of PNSs (Figure S6e), in particular their thickness. According to AFM images, the shape of the PNSs tends to a parallelogram, corroborating what has been found by TEM, and the average thickness of PNSs, derived from the analysis of line profilers obtained from PNSs, showed significantly smaller structures with thicknesses of only ∼8 nm (Figure S7c), corresponding to ∼16 unit cells and in agreement with the lateral size determined by size statistics based on the particle size distribution (Figure S7b). Furthermore, we also successfully obtained similar PNSs using nanocubes as building blocks in the same way, as displayed in Figure S8, showing the general feasibility of our approach. In addition, we design a comparative experiment in which a Teflon-lined stainless steel autoclave without a cover was used, and other reaction conditions were kept unchanged, intending to study the effect of pressure on self-assembly. However, no self-assembly occurred (Figure S9), which indicates that pressure is the key factor in driving the self-assembly of NPs into NPSs, consistent with previous reports.[33,37]

It is generally known that the surface of NCs affects the structure and properties of trihalide perovskites and plays a key role in the growth and assembly of their crystals. After being treated for 60 min under high ambient pressure, all NPs completely become NSs (Figure 2a). Because of the large surface area of PNSs, face-to-face self-assembly occurs. Some PNSs vanish, being gradually replaced by other PNSs, with increasing contrast, indicating gradually increased thickness (Figure S10). The coexistence of PNSs with different contrast in the image correspond to different thickness was supported by PL spectroscopy, in which the two emission peaks located at ∼642 and 659 nm were ascribed to PNSs of different thicknesses (Figure S11). After the self-assembly process is completed, nearly defect-free single-crystalline thick PNSs formed (Figure 2e), as evidenced by SAED and HRTEM images (Figure 2f-h). In this scenario, the majority of the ligands that coat the PNSs' surfaces are further released into the solution, as illustrated in Figure 2a, leading to the merging of the PNSs. It can be seen that step-like products formed (Figure 2c) after self-assembly of the PNSs (Figure 2b), which

https://dx.doi.org/10.1021/acs.jpclett.0c02747
J. Phys. Chem. Lett. 2020, 11, 9862–9868

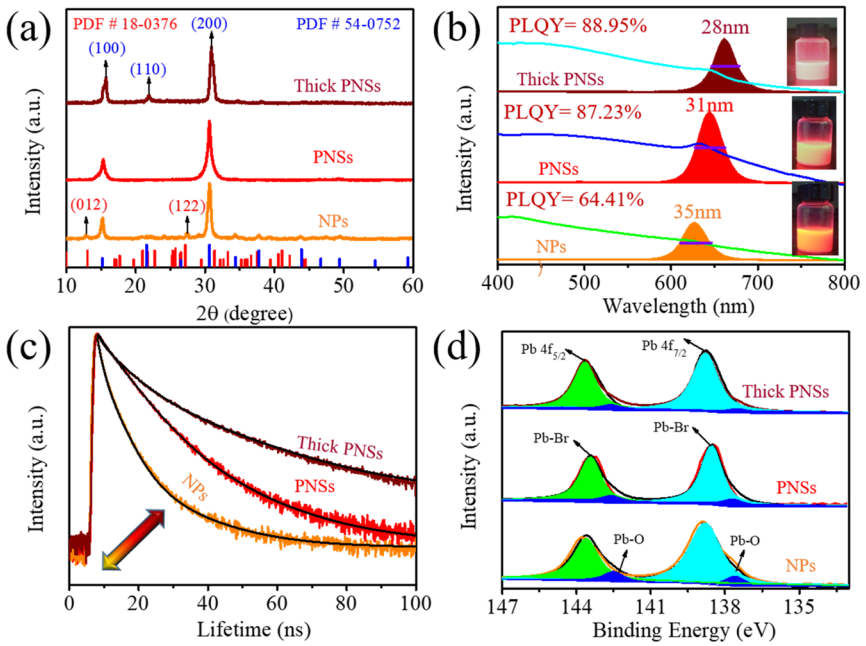

Figure 3. Sample characterization. (a) XRD patterns. (b) Optical absorption and steady-state PL spectra. (c) Time-resolution PL spectra. (d) High-resolution XPS spectra of Pb 4f.

further packed more closely into nanoassemblies (Figure 2d) and finally merged into well-defined thick PNSs with clear lattice fringes throughout the whole NS (Figure 2e), indicating high crystallinity. Because the fusion process is too fast, it is indeed difficult to capture consecutive images during the fusion process, but some coexisting prestage of thick PNSs composed of many thin PNSs can still be found, and the outline of the thin PNSs is clearly visible, suggesting that thick PNSs are indeed created from the thin PNSs (Figure S12). Thickness based on AFM measurements is ~40 nm (Figures 2i and S7d), which is nearly a 5-fold increase compared with that of the obtained shallow contrast. But other parameters, such as sides and angles, almost remain the same, in accordance with TEM results. It is well-known that ligands will adsorb on different facets of NCs, which will affect the self-assembled shape.[25] It is found that a small amount of oleic acid (0.5 mL) is beneficial to the formation of rectangular nanostructures, while an excess of oleic acid (1.5 mL) leads to larger nanostructure without well-defined morphology (Figure S13).

X-ray diffraction (XRD) data reveals that most of the peaks of NPs conform to standard cubic phase card, and several of them indicate the presence of orthorhombic phase (Figure 3a) (here, the crystal phase of $CsPbBrI_2$ is based on the standard card of the crystal phase of $CsPbBr_3$ as a reference). As reported previously by Rogach and co-workers,[32] cuboid-like NPs may belong to the cubic phase. Therefore, orthorhombic phase peaks probably originate from the phase transformation of NPs during storage, purification, or characterization, as confirmed by a previous report.[27] As assembly proceeds, the XRD patterns of characteristic peaks ascribed to the orthorhombic phase disappear, especially for the (012) and (122) crystal facets, while the peaks of cubic phase, such as the (110) crystal facets start to appear. When the product completely converts into thick PNSs, almost all peaks can be indexed as a pure cubic phase (Figure 3a). In the following section, a significant redshift can be observed for the continuous self-assembly process, which is good agreement with the size effect.[38] Accompanied by the redshift of PL peaks, their PL intensity increases at first and then decreases, but the final PL intensity is still 1.4 times that of the NPs (Figure 3b). Therefore, we believe that initial enhancement of PL is probably attributable to the disappearance of the grain boundaries between the adjacent NPs, but the subsequent weakening likely relates to a weak quantum confinement effect. It is clearly observed that PL lifetime gradually becomes longer with assembly (Figure 3c and Table S1). Because longer PL lifetime means larger charge diffusion distance before recombination within the perovskite crystal lattice, it is rational to say that PNSs have a much longer-scale ordered crystal lattice than that of small NPs.[31] X-ray photoelectron spectroscopy (XPS) further analyzes the properties of samples (Figure S14). In high-resolution XPS spectra of Pb 4f, Pb $4f_{7/2}$ and $4f_{5/2}$ can be fitted into two peaks, which demonstrate the existence of Pb−Br bonds and subsequent formation of Pb−O bonds, respectively.[39] It is clearly found that the Pb−O peaks, located at 137.78 and 142.61 eV, appeared to decrease with assembly (Figure 3d). The Br 3d peaks are fitted into high and low binding energy peaks, corresponding to the inner and surface bromine ions, respectively, as plotted in Figure S14c. Theoretically, thick PNSs possess fewer surface atoms than other samples. However, the intensity ratio of surface bromine to inner bromine is almost the same for all samples. This indicates that the surface of the thick PNSs changes from a Pb^0-rich state to a bromine-rich state and that in this process, nonradiative recombination on the surface is suppressed, which are in good agreement with enhanced PLQYs.[40]

As is well-known, the stability of perovskite NCs is a crucial issue, not only for the optoelectronic characterizations but also for their practical applications in solid-state devices. The stability of the samples was monitored by measuring their PL intensity, which has been frequently used in previous work.[41−43] Subsequently, a portable UV lamp generating an irradiance of 48 W was used as the light source to illuminate the sample. It can be found that after 24 h of UV illumination,

https://dx.doi.org/10.1021/acs.jpclett.0c02747
J. Phys. Chem. Lett. 2020, 11, 9862−9868

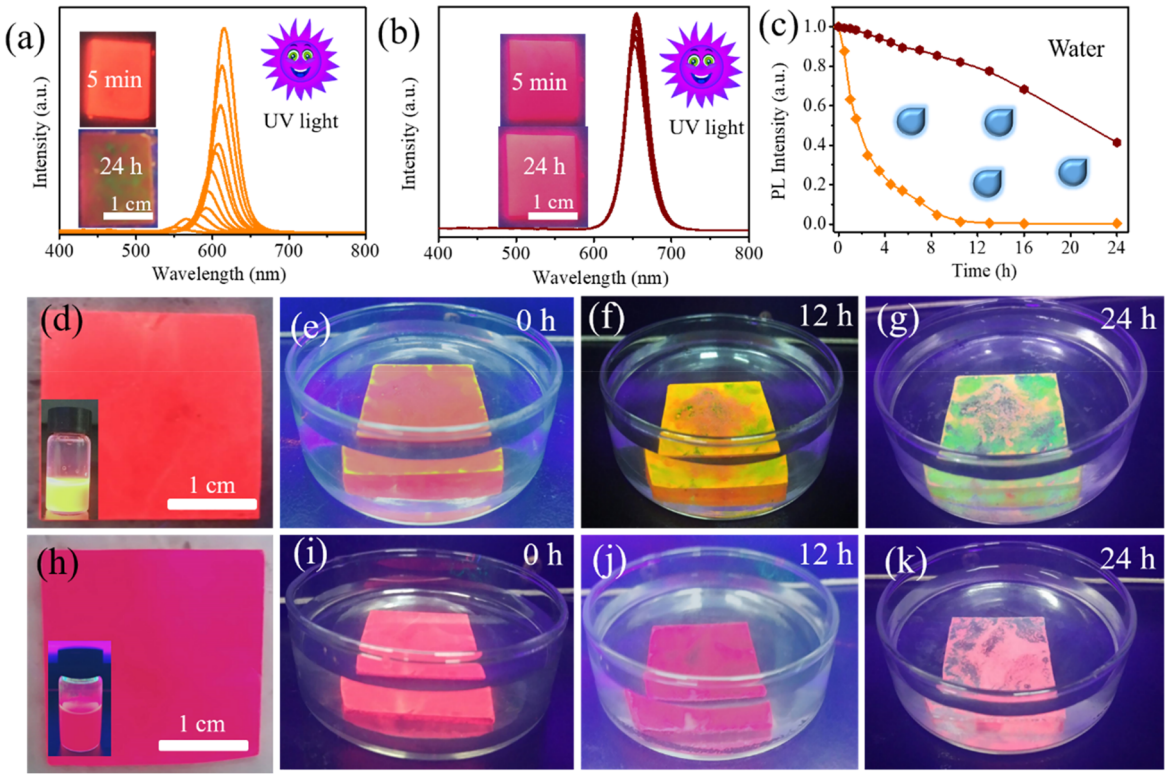

Figure 4. Stability of the samples against light and water is monitored by measuring their PL intensity. (a and b) Change of the PL intensity of both sample under UV light. (c) Comparison of relative PL intensity for the both samples in water. (d–k) Optical images of both sample immersed in water for different times.

the PL intensity of the NPs corresponding red emission becomes weak and almost disappears. By contrast, the emission intensity of the thick PNSs can maintain approximately 85% of the initial intensity after the same treatment, even 24 h (Figures 4a,b and S15), indicating that the thick PNSs have high stability against light. In addition, the thick PNSs have a larger contact angle compared with NP samples (Figure S16a,b), which can better resist water molecules. Subsequently, these samples were spin-coated on the glass to form a film and then immersed in water to monitor the fluorescence intensity. Although the fluorescence of the sample is gradually quenched by immersion in water, the fluorescence quenching of the thick PNSs is much slower than that of the NPs (Figure 4c). This may be because thick PNSs have higher crystallinity and minimize the surface area in comparison to NPs,[33,42] which makes it difficult for water molecules to enter the perovskite lattice along grain boundaries. In association with PL intensity, NPs correspond to the change in emission color from yellow-red to green, but the emission color of thick PNSs is almost unchanged (Figure 4d–k). This phenomenon indicates that thick PNSs not only have strong antiwater stability but also can resist the migration/redistribution of halide ions in the crystal lattice.[44] More importantly, thick PNSs retained the cubic phase throughout the testing period in water, but NPs had already partially converted to the orthorhombic phase within 12 h (Figure S16c,d). Not surprisingly, after 24 h, NPs almost completely transformed into the orthorhombic phase.

In summary, we demonstrate that pressure can induce the self-assembly of $CsPbBrI_2$ NPs into PNSs. The pressure-induced self-assembly mechanism for the PNSs is clearly illuminated by the monitoring of the shape evolution. More importantly, the stability and PL intensity of PNSs can be improved because of the disappearance of the grain boundaries and increased crystallinity. This facile synthesis method opens up a promising road for the synthesis of PNSs and guides the self-assembly of other nanostructures.

■ ASSOCIATED CONTENT

Supporting Information

The Supporting Information is available free of charge at https://pubs.acs.org/doi/10.1021/acs.jpclett.0c02747.

Synthesis of $CsPbBrI_2$ NPs and experimental details of self-assembly of NPs into PNSs under high pressure; characterization of the self-assembly process from NPs to PNSs by particle size distribution, TEM, and PL spectroscopy; characterization of the stability of NPs and PNSs by PL spectra, contact angle, and XRD pattern (PDF)

■ AUTHOR INFORMATION

Corresponding Author

Minqiang Wang − *Electronic Materials Research Laboratory, Key Laboratory of the Ministry of Education International Center for Dielectric Research, Shannxi Engineering Research Center of Advanced Energy Materials and Devices, Xi'an Jiaotong University, 710049 Xi'an, China*;
Email: mqwang@xjtu.edu.cn

Authors

Yongqiang Ji − *Electronic Materials Research Laboratory, Key Laboratory of the Ministry of Education International Center for Dielectric Research, Shannxi Engineering Research Center of Advanced Energy Materials and Devices, Xi'an Jiaotong*

https://dx.doi.org/10.1021/acs.jpclett.0c02747
J. Phys. Chem. Lett. 2020, 11, 9862−9868

University, 710049 Xi'an, China; orcid.org/0000-0002-0848-9643

Zhi Yang − *Electronic Materials Research Laboratory, Key Laboratory of the Ministry of Education International Center for Dielectric Research, Shannxi Engineering Research Center of Advanced Energy Materials and Devices, Xi'an Jiaotong University, 710049 Xi'an, China;* orcid.org/0000-0003-1499-6059

Hengwei Qiu − *Electronic Materials Research Laboratory, Key Laboratory of the Ministry of Education International Center for Dielectric Research, Shannxi Engineering Research Center of Advanced Energy Materials and Devices, Xi'an Jiaotong University, 710049 Xi'an, China*

Song Kou − *Electronic Materials Research Laboratory, Key Laboratory of the Ministry of Education International Center for Dielectric Research, Shannxi Engineering Research Center of Advanced Energy Materials and Devices, Xi'an Jiaotong University, 710049 Xi'an, China*

Muhammad Amin Padhiar − *Electronic Materials Research Laboratory, Key Laboratory of the Ministry of Education International Center for Dielectric Research, Shannxi Engineering Research Center of Advanced Energy Materials and Devices, Xi'an Jiaotong University, 710049 Xi'an, China*

Arshad Saleem Bhatti − *Centre for Micro and Nano Devices, Department of Physics, COMSATS Institute of Information Technology, Islamabad 44500, Pakistan*

Nikolai V. Gaponenko − *Belarusian State University of Informatics and Radioelectronics, 220013 Minsk, Belarus*

Complete contact information is available at: https://pubs.acs.org/10.1021/acs.jpclett.0c02747

Notes

The authors declare no competing financial interest.

■ ACKNOWLEDGMENTS

We thank Ms. Jiamei Liu at the Instrument Analysis Center of Xi'an Jiaotong University for her help with XPS analysis and Mr. Chuansheng Ma at International Center for Dielectric Research for help with TEM. This work was supported by the National Natural Science Foundation of China (NSFC, 61774124, 51572216, and 61604122), the Fundamental Research Funds for the Central Universities (1191329876 and 1191329152), the 111 Plan (B14040), the China Postdoctoral Science Foundation (2019M660253), the Natural Science Basic Research Program of Shannxi (No. 2019JLP-18), and the Innovation Capability Support Program of Shannxi (Nos. 2018PT-28 and 2019PT-05).

■ REFERENCES

(1) Protesescu, L.; Yakunin, S.; Bodnarchuk, M. I.; Krieg, F.; Caputo, R.; Hendon, C. H.; Yang, R. X.; Walsh, A.; Kovalenko, M. V. Nanocrystals of Cesium Lead Halide Perovskites ($CsPbX_3$, X = Cl, Br, and I): Novel Optoelectronic Materials Showing Bright Emission with Wide Color Gamut. *Nano Lett.* **2015**, *15*, 3692−3696.

(2) Zhang, F.; Zhong, H.; Chen, C.; Wu, X.; Hu, X.; Huang, H.; Han, J.; Zou, B.; Dong, Y. Brightly Luminescent and Color Tunable Colloidal $CH_3NH_3PbX_3$ (X = Br, I, Cl) Quantum Dots: Potential Alternatives for Display Technology. *ACS Nano* **2015**, *9*, 4533−4542.

(3) Zhang, X.; Wang, H.; Hu, Y.; Pei, Y.; Wang, S.; Shi, Z.; Colvin, V. K.; Wang, S.; Zhang, Y.; Yu, W. W. Strong Blue Emission from Sb^{3+}-Doped Super Small $CsPbBr_3$ Nanocrystals. *J. Phys. Chem. Lett.* **2019**, *10*, 1750−1756.

(4) Ji, Y.; Wang, M.; Yang, Z.; Ji, S.; Qiu, H.; Gaponenko, N. V. Reversible Transformation Between $CsPbBr_3$ Nanowires and Nanoparticles. *Chem. Commun.* **2019**, *55*, 12809−12812.

(5) Akkerman, Q. A.; Raino, G.; Kovalenko, M. V.; Manna, L. Genesis, Challenges and Opportunities for Colloidal Lead Halide Perovskite Nanocrystals. *Nat. Mater.* **2018**, *17*, 394−405.

(6) Zhou, Q.; Bai, Z.; Lu, W.; Wang, Y.; Zou, B.; Zhong, H. In Situ Fabrication of Halide Perovskite Nanocrystal Embedded Polymer Composite Films with Enhanced Photoluminescence for Display Backlights. *Adv. Mater.* **2016**, *28*, 9163−9168.

(7) Pan, A.; Ma, X.; Huang, S.; Wu, Y.; Jia, M.; Shi, Y.; Liu, Y.; Wangyang, P.; He, L.; Liu, Y. $CsPbBr_3$ Perovskite Nanocrystal Grown on MXene Nanosheets for Enhanced Photoelectric Detection and Photocatalytic CO_2 Reduction. *J. Phys. Chem. Lett.* **2019**, *10*, 6590−6597.

(8) Zhang, L.; Yuan, F.; Dong, H.; Jiao, B.; Zhang, W.; Hou, X.; Wang, S.; Gong, Q.; Wu, Z. One-Step Co-Evaporation of All-Inorganic Perovskite Thin Films with Room-Temperature Ultralow Amplified Spontaneous Emission Threshold and Air Stability. *ACS Appl. Mater. Interfaces* **2018**, *10*, 40661−40671.

(9) Huang, Z. P.; Ma, B.; Wang, H.; Li, N.; Liu, R.-T.; Zhang, Z.-Q.; Zhang, X.-D.; Zhao, J.-H.; Zheng, P.-Z.; Wang, Q.; Zhang, H.-L. In Situ Growth of 3D/2D ($CsPbBr_3$/$CsPb_2Br_5$) Perovskite Heterojunctions Toward Optoelectronic Devices. *J. Phys. Chem. Lett.* **2020**, *11*, 6007−6015.

(10) Han, B.; Imran, M.; Zhang, M.; Chang, S.; Wu, X.; Zhang, X.; Tang, J.; Wang, M.; Ali, S.; Li, X.; Yu, G.; Han, J.; Wang, L.; Zou, B.; Zhong, H. Efficient Light-Emitting Diodes Based on in Situ Fabricated $FAPbBr_3$ Nanocrystals: The Enhancing Role of the Ligand-Assisted Reprecipitation Process. *ACS Nano* **2018**, *12*, 8808−8816.

(11) Sanehira, E. M.; Marshall, A. R.; Christians, J. A.; Harvey, S. P.; Ciesielski, P. N.; Wheeler, L. M.; Schulz, P.; Lin, L. Y.; Beard, M. C.; Luther, J. M. Enhanced Mobility $CsPbI_3$ Quantum Dot Arrays for Record-Efficiency High-Voltage Photovoltaic Cells. *Sci. Adv.* **2017**, *3*, eaao4204.

(12) Shi, E.; Gao, Y.; Finkenauer, B. P.; Akriti; Coffey, A. H.; Dou, L. Two-dimensional Halide Perovskite Nanomaterials and Heterostructures. *Chem. Soc. Rev.* **2018**, *47*, 6046−6072.

(13) Yang, S.; Wang, Y.; Liu, P.; Cheng, Y. B.; Zhao, H. J.; Yang, H. G. Functionalization of Perovskite Thin Films with Moisture Tolerant Molecules. *Nat. Energy.* **2016**, *1*, 15016−15022.

(14) Zhang, J.; Zhang, L.; Cai, P.; Xue, X.; Wang, M.; Zhang, J.; Tu, G. Enhancing Stability of Red Perovskite Nanocrystals through Copper Substitution for Effcient Light-emitting Diodes. *Nano Energy* **2019**, *62*, 434−441.

(15) Ravi, V. K.; Santra, P. K.; Joshi, N.; Chugh, J.; Singh, S. K.; Rensmo, H.; Ghosh, P.; Nag, A. Origin of the Substitution Mechanism for the Binding of Organic Ligands on the Surface of $CsPbBr_3$ Perovskite Nanocubes. *J. Phys. Chem. Lett.* **2017**, *8*, 4988−4994.

(16) Yang, Z.; Wang, M.; Qiu, H.; Yao, X.; Lao, X.; Xu, S.; Lin, Z.; Sun, L.; Shao, J. Engineering the Exciton Dissociation in Quantum-Confined 2D $CsPbBr_3$ Nanosheet Films. *Adv. Funct. Mater.* **2018**, *28*, 1705908.

(17) Lao, X.; Yang, Z.; Su, Z.; Wang, Z.; Ye, H.; Wang, M.; Yao, X.; Xu, S. Luminescence and Thermal Behaviors of Free and Trapped Excitons in Cesium Lead Halide Perovskite Nanosheets. *Nanoscale* **2018**, *10*, 9949−9956.

(18) Shamsi, J.; Dang, Z.; Bianchini, P.; Canale, C.; Di Stasio, F.; Brescia, R.; Prato, M.; Manna, L. Colloidal Synthesis of Quantum Confined Single Crystal $CsPbBr_3$ Nanosheets with Lateral Size Control up to the Micrometer Range. *J. Am. Chem. Soc.* **2016**, *138*, 7240−7243.

(19) Bekenstein, Y.; Koscher, B. A.; Eaton, S. W.; Yang, P.; Alivisatos, A. P. Highly Luminescent Colloidal Nanoplates of Perovskite Cesium Lead Halide and Their Oriented Assemblies. *J. Am. Chem. Soc.* **2015**, *137*, 16008−16011.

(20) Huang, H.; Raith, J.; Kershaw, S. V.; Kalytchuk, S.; Tomanec, O.; Jing, L.; Susha, A. S.; Zboril, R.; Rogach, A. L. Growth Mechanism of Strongly Emitting $CH_3NH_3PbBr_3$ Perovskite Nanocrystals with a Tunable Bandgap. *Nat. Commun.* **2017**, *8*, 996.
(21) Peng, L.; Dutta, A.; Xie, R.; Yang, W.; Pradhan, L. Dot-Wire-Platelet-Cube: Step Growth and Structural Transformations in $CsPbBr_3$ Perovskite Nanocrystals. *ACS Energy Lett.* **2018**, *3*, 2014−2020.
(22) Zhang, X.; Lv, L.; Ji, L.; Guo, G.; Liu, L.; Han, D.; Wang, B.; Tu, Y.; Hu, J.; Yang, D.; Dong, A. Self-Assembly of One-Dimensional Nanocrystal Superlattice Chains Mediated by Molecular Clusters. *J. Am. Chem. Soc.* **2016**, *138*, 3290−3293.
(23) Balakrishnan, S. K.; Kamat, P. V. Ligand Assisted Transformation of Cubic $CsPbBr_3$ Nanocrystals into Two-Dimensional $CsPb_2Br_5$ Nanosheets. *Chem. Mater.* **2018**, *30*, 74−78.
(24) Tong, Y.; Yao, E. P.; Manzi, A.; Manzi, A.; Bladt, E.; Wang, K.; Döblinger, M.; Bals, S.; Müller-Buschbaum, P.; Urban, A. S.; Polavarapu, L.; Feldmann, J. Spontaneous Self-Assembly of Perovskite Nanocrystals into Electronically Coupled Supercrystals: Toward Filling the Green Gap. *Adv. Mater.* **2018**, *30*, 1801117.
(25) Ji, Y.; Wang, M.; Yang, Z.; Ji, S.; Qiu, H. Nanowire-Assisted Self-Assembly of One Dimensional Nanocrystal Superlattice Chains. *J. Mater. Chem. C* **2019**, *7*, 8471−8476.
(26) Li, B. Y.; Li, Y. C.; Lu, Z. Y. Spontaneous Formation of Moiré Patterns through Self-Assembly of Janus Nanoparticles. *J. Phys. Chem. Lett.* **2020**, *11*, 4542−4547.
(27) Sun, J. K.; Huang, S.; Liu, X. Z.; Xu, Q.; Zhang, Q. H.; Jiang, W. J.; Xue, D. J.; Xu, J. C.; Ma, J. Y.; Ding, J.; Ge, Q. Q.; Gu, L.; Fang, X. H.; Zhong, H. Z.; Hu, J. S.; Wan, L. J. Polar Solvent Induced Lattice Distortion of Cubic $CsPbI_3$ Nanocubes and Hierarchical Self-Assembly into Orthorhombic Single-Crystalline Nanowires. *J. Am. Chem. Soc.* **2018**, *140*, 11705−11715.
(28) Dang, Z.; Dhanabalan, B.; Castelli, A.; Dhall, R.; Bustillo, K. C.; Marchelli, D.; Spirito, D.; Petralanda, U.; Shamsi, J.; Manna, L.; Krahne, R.; Arciniegas, M. P. Temperature Driven Transformation of $CsPbBr_3$ Nanoplatelets into Mosaic Nanotiles in Solution through Self-Assembly. *Nano Lett.* **2020**, *20*, 1808−1818.
(29) Liu, J.; Song, K.; Shin, Y.; Liu, X.; Chen, J.; Yao, K. X.; Pan, J.; Yang, C.; Yin, J.; Xu, L. J.; Yang, H.; El-Zohry, A. M.; Xin, B.; Mitra, S.; Hedhili, M. N.; Roqan, I. S.; Mohammed, O. F.; Han, Y.; Bakr, O. M. Light-Induced Self-Assembly of Cubic $CsPbBr_3$ Perovskite Nanocrystals into Nanowires. *Chem. Mater.* **2019**, *31*, 6642−6649.
(30) Dang, Z.; Shamsi, J.; Palazon, F.; Imran, M.; Akkerman, Q. A.; Park, S.; Bertoni, G.; Prato, M.; Brescia, R.; Manna, L. In Situ Transmission Electron Microscopy Study of Electron Beam Induced Transformations in Colloidal Cesium Lead Halide Perovskite Nanocrystals. *ACS Nano* **2017**, *11*, 2124−2132.
(31) Li, H.; Liu, X.; Ying, Q.; Wang, C.; Jia, W.; Xing, X.; Yin, L.; Lu, Z.; Zhang, K.; Pan, Y.; Shi, Z.; Huang, L.; Jia, D. Self-Assembly of Perovskite $CsPbBr_3$ Quantum Dots Driven by a Photo-Induced Alkynyl Homocoupling Reaction. *Angew. Chem., Int. Ed.* **2020**, *59*, 17207.
(32) Bi, C.; Wang, S.; Kershaw, S. V.; Zheng, K.; Pullerits, T.; Gaponenko, S.; Tian, J.; Rogach, A. L. Spontaneous Self-Assembly of Cesium Lead Halide Perovskite Nanoplatelets into Cuboid Crystals with High Intensity Blue Emission. *Adv. Sci.* **2019**, *6*, 1900462.
(33) Nagaoka, Y.; Hills-Kimball, K.; Tan, R.; Li, R.; Wang, Z.; Chen, O. Nanocube Superlattices of Cesium Lead Bromide Perovskites and Pressure-Induced Phase Transformations at Atomic and Mesoscale Levels. *Adv. Mater.* **2017**, *29*, 1606666.
(34) Udayabhaskararao, T.; Kazes, Z.; Houben, L.; Lin, H.; Oron, D. Nucleation, Growth, and Structural Transformations of Perovskite Nanocrystals. *Chem. Mater.* **2017**, *29*, 1302−1308.
(35) Lian, L.; Zhai, G.; Cheng, F.; Xia, Y.; Zheng, M.; Ke, J.; Gao, M.; Liu, H.; Zhang, D.; Li, L.; Gao, J.; Tang, J.; Zhang, J. Colloidal Synthesis of Lead-Free All-Inorganic Cesium Bismuth Bromide Perovskite Nanoplatelets. *CrystEngComm* **2018**, *20*, 7473−7478.
(36) Zhang, H.; Liao, Q.; Wu, Y.; Chen, J.; Gao, Q.; Fu, H. Pure Zero-Dimensional Cs_4PbBr_6 Single Crystal Rhombohedral Microdisks with High Luminescence and Stability. *Phys. Chem. Chem. Phys.* **2017**, *19*, 29092−29098.
(37) Zhang, L.; Zeng, Q.; Wang, K. Pressure-Induced Structural and Optical Properties of Inorganic Halide Perovskite $CsPbBr_3$. *J. Phys. Chem. Lett.* **2017**, *8*, 3752−3758.
(38) Liu, L.; Zhao, R.; Xiao, C.; Zhang, F.; Pevere, F.; Shi, K.; Huang, H.; Zhong, H.; Sychugov, Il. Size-Dependent Phase Transition in Perovskite Nanocrystals. *J. Phys. Chem. Lett.* **2019**, *10*, 5451−5457.
(39) Wu, Y.; Wei, C.; Li, X.; Li, Y.; Qiu, S.; Shen, W.; Cai, B.; Sun, Z.; Yang, D.; Deng, Z.; Zeng, H. In Situ Passivation of $PbBr_6^{4-}$ Octahedra toward Blue Luminescent $CsPbBr_3$ Nanoplatelets with Near 100% Absolute Quantum Yield. *ACS Energy Lett.* **2018**, *3*, 2030−2037.
(40) Ji, Y.; Wang, M.; Yang, Z.; Qiu, H.; Dou, J.; Ji, S.; Gaponenko, N. V. Highly Stable Na: $CsPb(Br,I)_3@Al_2O_3$ Nanocomposites Prepared by a Pre-protection Strategy. *Nanoscale* **2020**, *12*, 6403−6410.
(41) Pan, A.; Wang, J.; Jurow, M. J.; Jia, M.; Liu, Y.; Wu, Y.; Zhang, Y.; He, L.; Liu, Y. A General Strategy for the Preparation of Stable Luminous Nanocomposite Inks Using Chemically Addressable $CsPbX_3$ Peroskite Nanocrystals. *Chem. Mater.* **2018**, *30*, 2771−2780.
(42) Wang, W.; Wang, D.; Fang, F.; Wang, S.; Xu, G.; Zhang, T. $CsPbBr_3/Cs_4PbBr_6$ Nanocomposites: Formation Mechanism, Large-scale and Green Synthesis, and Application in White Light-Emitting Diodes. *Cryst. Growth Des.* **2018**, *18*, 6133−6141.
(43) Wang, C.; Chesman, A. S. R.; Jasieniak, J. J. Stabilizing the Cubic Perovskite Phase of $CsPbI_3$ Nanocrystals by Using an Alkyl Phosphinic Acid. *Chem. Commun.* **2017**, *53*, 232−235.
(44) Fan, W.; Shi, Y.; Shi, T.; Chu, S.; Chen, W.; Ighodalo, K. O.; Zhao, J.; Li, X.; Xiao, Z. Suppression and Reversion of Light-Induced Phase Separation in Mixed-Halide Perovskites by Oxygen Passivation. *ACS Energy Lett.* **2019**, *4*, 2052−2058.

https://dx.doi.org/10.1021/acs.jpclett.0c02747
J. Phys. Chem. Lett. 2020, 11, 9862−9868